Effect of in situ annealing on the structural and electrical properties and infrared photodetection of III-Sb on GaAs using interfacial misfit array

Bo Wen Jia, Kian Hua Tan, Wan Khai Loke, Satrio Wicaksono, and Soon Fatt Yoon

School of Electrical and Electronic Engineering, Nanyang Technological University, Nanyang Avenue, Singapore 639798, Republic of Singapore

Abstract

This work presents the effects of in situ thermal annealing under antimony overpressure on the structural, electrical, and optical properties of III-Sb (GaSb and InSb) grown on (100) GaAs using an interfacial misfit array to accommodate the lattice mismatch. Both the sample growth and the in situ thermal annealing were carried out in the in the molecular beam epitaxy, and the temperature of the as-grown sample was increased to excess its growth temperature during the annealing. X-ray diffraction demonstrates nearly fully relaxed as-grown and annealed III-Sb layers. The optimal annealing temperatures and durations are for 590°C, 5 minutes for GaSb and 420°C, 15 minutes for InSb, respectively. In situ annealing decreased the surface roughness of the III-Sb layers. X-ray reciprocal space mapping and transmission electron microscopy observation showed stable interfacial misfit arrays, and no interfacial diffusion occurred in the annealed III-Sb layers. A Hall measurement of unintentionally doped III-Sb layers showed greater carrier mobility and a lower carrier concentration in the annealed samples at both 77 and 300 K. In situ annealing improved the photoresponsivity of GaSb and InSb photoconductors grown on GaAs in the near- and mid-infrared ranges, respectively.

1. Introduction

III-antimonide–based compound semiconductors (GaSb and InSb) are well-established materials for applications in high-electron-mobility transistors (HEMTs), photodetectors, lasers, and solar cells due to their high carrier mobility and small direct band gap [1]. A GaSb photodetector exhibits a cutoff wavelength of approximately 1.6 μm due to its band gap energy of 0.726 eV [2]. InSb photodetectors are conventionally cooled to 77 K to decrease dark current. At that temperature, the

band gap energy of InSb is 0.23 eV, which enables the detection of light at infrared wavelengths up to 5.5 μm [3]. Monolithic integration of III-Sb devices on GaAs could benefit from the greater resistivity, lower price, and larger size of commercially available (100) GaAs substrates, which may result in greater speed, superior performance, and enhanced functionality of devices [4, 5]. Moreover, GaAs-based read-out integrated circuits and III-Sb-based photodetectors can be integrated via heteroepitaxial growth of III-Sb on GaAs without the use of a bonding process [6]. This development may also allow the integration of III-Sb devices on Si substrate because of the sophisticated development of the growth of GaAs/Ge on a Si substrate [7, 8].

The heteroepitaxial growth of III-Sb on GaAs promotes a high density of dislocation defects in the layers because of the high level of lattice mismatch (7.83% for GaSb/GaAs and 14.61% for InSb/GaAs). The use of an interfacial misfit (IMF) array to accommodate lattice mismatch is an emerging approach to growing high-quality lattice mismatch layers without a thick buffer [9, 10]. Transmission electron microscopy (TEM) was used to observe that the IMF array consisted of periodically distributed 90° misfit dislocations at the GaSb/GaAs and InSb/GaAs interfaces [9]. The growth of GaSb on GaAs using IMF array photonic devices has been reported [11, 12]. Our previous reports described the optimization of the growth temperature [4, 13] and pre-growth Sb reconstruction on the GaAs surface [14] in the growth of III-Sb on a (100) GaAs substrate to increase the uniformity of the IMF array. The carrier mobility in those III-Sb layers is half that in bulk III-Sb. Further suppression of threading dislocation is still required, especially for application in HEMTs and photodetectors. Dislocations reduce the carrier mobility, which is essential in HEMTs [15]. They also increase the dark current of photodetectors, which leads to deteriorating detection capability [16]. Therefore, techniques used to reduce threading dislocation, such as thermal annealing, are required. Thermal annealing has been widely used in heteroepitaxy, such as Ge/Si [16, 17], GaAs/Si [18], HgCdTe/Si [19], and GaP/GaAs [20], to suppress threading dislocation and improve device performance. The high temperature of the annealing process has resulted in annihilation and coalescence of threading dislocations [19]. An appropriate annealing process should be investigated to reduce the density of threading dislocation without disrupting the stability of the IMF array at the III-Sb/GaAs interface. Previous research of annealing on GaSb grown on GaAs using IMF array was based on ex situ annealing process and focused on the reduction of interfacial states rather than improving the quality of the layer [21, 22]. Applying in situ annealing using molecular beam epitaxy (MBE) system on GaSb and InSb grown on GaAs

using IMF array is rarely reported. Recently, some p-i-n and nBn photodetectors been developed on GaAs using IMF array and demonstrated a comparable detectivity with the device on native substrate [11, 23, 24]. These photodetectors are only based on 6.1 Å family compound semiconductors (InAs, GaSb, AlSb and their alloys) and their lattice mismatch with GaAs is about 7.83%. The lattice mismatch between InSb and GaAs is 14.61% and the InSb devices grown on GaAs using IMF array has not been developed. A GaSb or InSb photoconductive photodetector (photoconductor) can detect near- or mid-infrared and demonstrate similar spectral response like photodiode [25]. Its responsivity depends on the minority carrier mobility and life time of semiconductor which can be improved through decreasing the density of dislocations after annealing [26, 27]. Therefore, the responsivity of III-Sb photoconductor can be used to evaluate the effect of annealing. In addition, the simple growth and fabrication process of photoconductor avoid other factors affect the performance of detectors. Therefore, the effects of in situ annealing on III-Sb grown on GaAs using an IMF array and its effect on the performance of photoconductors were investigated.

In this study, GaSb and InSb layers were first grown on GaAs using an IMF array by MBE. In situ annealing was carried out after the growth of the 125 nm GaSb and 100 nm InSb layers, which are referred to as “buffer layers” in this paper. After annealing, the photoconductor structure was grown. This arrangement minimizes the effects of the annealing process on the device layer, which may consist of superlattice and doping layers. The structural and electrical properties of annealed and as-grown III-Sb/GaAs samples were investigated, and photoconductors based on III-Sb/GaAs were fabricated to measure the photoresponse.

2. Experimental procedure

GaSb and InSb layers were grown on (100) GaAs substrates using a solid-source MBE system equipped with arsenic (As) and antimony (Sb) valved crackers to provide As_2 and Sb_2. After oxide desorption at 580 °C, a 100 nm thick GaAs layer was grown on the GaAs substrate to achieve a smooth GaAs surface. The excess absorbed As on the GaAs surface was then removed at 540 °C by terminating the As flux supply for 10 minutes. The temperature was lowered to 500 °C, and the samples were exposed to Sb_2 flux with a beam-equivalent flux of about 1.2×10^{-6} Torr. After 4 minutes of Sb flux exposure, a clear (2 × 8) pattern was observed on reflection high-energy electron

diffraction (RHEED), indicating that a (2 × 8) Sb reconstruction had formed on the GaAs surface. The temperature of the substrate was then lowered to the growth temperature at 30°C/min. During the cooling process, the Sb valve was closed and the RHEED pattern was maintained at (2 × 8) reconstruction.

Fig. 1 is a schematic diagram of the photoconductors, which consisted of top interdigitate electrodes and the heterostructures of III-Sb on GaAs. As shown in Fig. 1, the III-Sb buffer layers were first grown on the GaAs surface. GaSb buffer (125 nm) was grown at 390 °C, and InSb buffer (100 nm) was grown at 310 °C. Information about the growth of III-Sb on GaAs using an IMF array has been given in detail elsewhere [4, 13]. During annealing, a high temperature resulted in a high motion velocity of dislocations [28], thus, a higher probability of the annihilation of dislocations. However, the surface of GaSb and InSb is roughed due to surface Sb re-evaporation at too high temperature [29]. Before in situ annealing, the temperature of GaSb or InSb was increased under Sb overpressure until the RHEED patterns disappeared. The disappearance of RHEED pattern indicated a fully disordered surface of III-Sb layers caused by Sb re-evaporation. The temperature 10°C below the temperature at which the RHEED pattern vanished was determined as the annealing temperature for GaSb or InSb on GaAs. In situ annealing was carried out at 590°C for GaSb and 420°C for InSb for different durations (5, 10, 15, and 30 minutes) in the MBE chamber and exposed to Sb_2 flux with a beam-equivalent flux of about 1.2×10^{-6} Torr. The rate of ramp up and down were fixed at 30 °C/min. The ramp up and down were monitored using RHEED and a clear (1×3) pattern was kept during the ramp up and down indicating a flat surface. After annealing, 300 nm of GaSb and 600 nm of InSb were grown at 390°C and 310°C, respectively. To ensure the effects of annealing, a 425 nm GaSb layer and a 700 nm InSb layer were grown on the GaAs without annealing as a control group.

After MBE growth, the x-ray ω-2θ scan, ω scan, and reciprocal space map (RSM) were obtained using an x-ray diffractometer with a beam collimator and analyzer crystals to achieve sufficiently high resolution. The surface morphology was measured by atomic force microscopy (AFM), and the interfacial microstructures were examined by cross-sectional TEM. Hall/Van der Pauw measurement was used to evaluate carrier motilities and concentrations. Interdigitated Au/Ti (80 nm/30 nm) electrodes were formed on the surface of samples using the standard photolithography, electron beam evaporation, and metal lift-off fabrication techniques. Near-infrared

photoresponsivity was measured with a xenon lamp in conjunction with a monochromator. A tunable laser and a 700°C black body radiation source were used for mid-infrared photoresponsivity measurement. The InSb photoconductors were mounted on a liquid-nitrogen-cooled optical cryostat for measurements below 300 K.

3. Results and discussion

Table 1

Lattice constant, relaxation, (004) rocking curve FWHM, and surface roughness for GaSb/GaAs and InSb/GaAs grown with different annealing times.

Structure	Annealing time (minute)	$a_{\perp}$ (Å)	$a_{//}$ (Å)	Relaxation (%)	(004) rocking curve FWHM (arcsec)	Root mean square roughness (nm)
GaSb on GaAs	0	6.101	6.093	99.4	498	1.6
	5	6.100	6.094	99.6	471	0.9
	10	6.103	6.092	99.1	474	1.1
	15	6.104	6.091	98.9	484	0.9
	30	6.099	6.094	99.6	489	1.0
InSb on GaAs	0	6.484	6.471	99.0	540	1.8
	5	6.480	6.475	99.5	528	1.1
	10	6.487	6.472	99.1	515	0.9
	15	6.482	6.476	99.6	507	1.0
	30	6.480	6.478	99.8	526	1.0

Symmetric (004) ω-2θ scans of the GaSb and InSb on GaAs with different annealing durations are shown in Figs. 2(a) and (b). The position of the GaAs peaks in the samples is normalized to 0°, and the annealing durations of the samples are indicated above the curves. The diffraction peaks of GaSb and GaAs can be observed in Fig. 2(a). No other obvious peak signal is observed between these two peaks, which indicates the absence of an intermediate layer between the III-Sb layers and the substrates. The GaSb peaks of all of the samples are located at the same position, and different annealing durations do not change the position of the GaSb peaks. Similar results are also found in the symmetric (004) XRD measurement of InSb on the GaAs samples, as shown in Fig. 2(b). The perpendicular and parallel lattice constants ($a_{\perp}$ and $a_{//}$) of the III-Sb layers, which were extracted from the symmetric (004) and asymmetric (115) ω-2θ scans (not presented here), are listed in Table 1. The degrees of relaxation in the GaSb and InSb layers are calculated using parallel

lattice constants and are also listed in Table 1. The GaSb and InSb layers in all of the samples are nearly 100% relaxed. The influence of the annealing duration on the degree of relaxation is not obvious.

The presence of threading dislocations broadens the full-width-half-maximum (FWHM) of the symmetric ω scan (rocking curve) [30, 31]. Therefore, the FWHM of a (004) ω scan were measured to qualitatively compare the threading dislocation density of the samples. Fig. 1(c) shows the relationship between the FWHM of the (004) ω scans and the annealing duration in the III-Sb layers. The values of FWHM are also listed in Table 1. The annealing process effectively reduced the FWHM of the samples' III-Sb peak. The optimal annealing durations were 5 minutes and 15 minutes for the GaSb and InSb layers, respectively. The quality of the III-Sb layer deteriorated when the samples were annealed for longer than the optimal duration. One possible explanation is that the long annealing process could have changed the IMF array at the III-Sb/GaAs interfaces, resulting in the formation of a non-uniform IMF array and threading dislocations [13, 32].

Figs. 3(a) and (b) show the annealing duration-dependent root mean square surface roughness of the III-Sb layers. The insets are the AFM surface images of the samples. The root mean square roughness values of the samples are listed in Table 1. All of the GaSb/GaAs samples showed a smooth surface, and the annealing process slightly decreased the surface roughness, as shown in Fig. 3(a). The annealed GaSb layers exhibited a root mean square roughness of approximately 1.0 nm over a 20 μm×20 μm area. A longer annealing duration did not further decrease the roughness. As shown in Fig. 3(b), the surface roughness of the InSb/GaAs samples illustrated characteristics similar to those of the GaSb/GaAs samples. The annealed InSb layers exhibited a root mean square roughness of approximately 1.0 nm over a 20 μm×20 μm area. The roughness of the as-grown sample was 1.8 nm. No obvious defects or steps were observed in the AFM images of InSb/GaAs. The annealing process decreased the surface roughness of the III-Sb layers. However, the effects of a different annealing duration on the surface roughness were not obvious. This result could be attributed to the diffusion of surface atoms during the annealing process [33].

A previous study suggested that annealing could result in interfacial diffusion and rearrangement of IMF dislocations [34]. In this study, III-Sb grown on GaAs using an IMF array exhibited a high density of misfit dislocations, which were uniformly distributed along the interface to relieve the

strain energy induced by the considerable lattice mismatch. Changes in the type of separation between the misfit dislocations could promote the formation of threading dislocations [13]. Therefore, x-ray RSMs of the samples were measured to investigate the possibility of interfacial diffusion. The diffusion at the III-Sb/interface formed a mixture of III-Sb and GaAs, which was probably a metamorphic buffer in heteroepitaxy. The metamorphic buffer could have been tilted to the orientation of the GaAs substrate, which could not be detected by (004) ω-2θ scanning, whereas the tilted buffer could be presented in an asymmetric RSM in a wafer-scale [35]. Furthermore, cross-sectional TEM was applied to observe the microstructures of IMF dislocations. Figs. 4(a) and (b) show the TEM images of GaSb on GaAs with 5 minutes of annealing at different magnifications. A sharp GaSb/GaAs interface is observed in Fig. 4(a), and black dots are distributed along this interface. If the entire strain energy was relieved solely by the IMF array, then the separation (S) of the adjacent dislocations can be calculated using the following formula [32]:

$$S = \frac{b}{f} \tag{1}$$

where b is the Burger vector of a 90° misfit dislocation and f is the lattice mismatch. The calculated separations are 5.51 nm for the GaSb/GaAs interface and 3.14 nm for the InSb/GaAs interface. A high-resolution TEM image at the interface is shown in Fig. 4(b), and black spots are distributed along the interface. Previous research confirmed that one black spot was a misfit dislocation in III-Sb on GaAs [9, 36] caused by the strain field induced by chemical bonds bending in misfit dislocations [37]. The separations between two adjacent dislocations were measured at 5.5 nm, which agreed well with the calculated value. These TEM observations were consistent with the observations of as-grown GaSb/GaAs demonstrated in a previous report [4]. Fig. 4(c) shows the (115) RSM of the same sample, in which the diagonal and vertical dashed lines indicate the reciprocal lattice peaks for fully relaxed and fully strained GaSb layers, respectively. The GaSb layer peak of the annealed sample is located at the diagonal dashed line, indicating that the layer was nearly fully relaxed. Fig. 4(c) shows only two distinguishing GaSb and GaAs substrate peaks in the RSM, which clearly implies that no metamorphic buffer structure induced by interfacial diffusion was formed in the annealed sample.

The TEM images of the InSb/GaAs interface after 15 minutes of annealing are shown in Figs. 5(a) and (b). The InSb/GaAs interface is sharp and includes black spots, indicating the presence of

misfit dislocations uniformly distributed along the interface [36]. Compared with misfit dislocations observed at the GaSb/GaAs interface, the two adjacent dislocations in InSb/GaAs are closer together (3.2 nm) due to the greater lattice mismatch. This separation agrees with the calculated value mentioned earlier.

Fig. 5(c) shows the (115) RSM of the same sample, indicating that the InSb layer was nearly 100% relaxed. No metamorphic buffer structure was observed. The results shown in Figs. 4 and 5 indicate that the IMF arrays of annealed III-Sb on GaAs samples were stable, with misfit dislocations uniformly distributed along the interfaces. The distances between the dislocations did not change, and no interfacial diffusion was seen. Compared with as-grown III-Sb layers on GaAs, the annealed samples remained nearly 100% relaxed, which further supported the observation of a stable IMF array after annealing because the rearrangement in the IMF dislocation inevitably influenced the relaxation of the layers [38].

Table 2

300-K and 77-K carrier mobility and concentration of III-Sb on GaAs with different annealing durations.

Material	Annealing time (min)	300 K carrier mobility (cm^2/Vs)	300 K carrier concentration (cm^{-3})	77 K carrier mobility (cm^2/Vs)	77 K carrier concentration (cm^{-3})
GaSb*	0	475	5.38×10^{16}	2,782	5.58×10^{15}
	5	503	5.05×10^{16}	2,880	4.87×10^{15}
InSb#	0	24320	2.61×10^{16}	2,541	2.02×10^{16}
	15	29040	2.27×10^{16}	3,608	1.21×10^{16}

* The GaSb layers grown on GaAs in this study are unintentionally p-type.
# The InSb layers grown on GaAs in this study are unintentionally n-type.

GaSb and InSb materials are importantly applied as a channel material for HEMTs because of their high hole (GaSb) and electron (InSb) mobility. A high density of threading dislocation suppresses the carrier mobility of a semiconductor layer [27]. Therefore, the effect of annealing on the threading dislocation density can be qualitatively compared by measuring the carrier mobility of III-Sb layers. In this study, both the GaSb and InSb layers were unintentionally doped. The influence of the GaAs substrate was negligible because of its semi-insulating nature. The carrier mobilities and concentrations of the III-Sb layers at 77 and 300 K are listed in Table 2. The 77 K

mobilities in the GaSb layers were higher than the 300 K mobilities due to weaker phonon scattering. In contrast, the carrier concentration at 77 K was lower than that at 300 K due to the higher thermal activation at higher temperatures.

The annealed GaSb layer exhibited a higher hole mobility and lower concentration than the as-grown sample at 300 K. The threading dislocations in unintentionally doped GaSb acted as acceptors to increase the hole concentration [39]. Moreover, they reduced the hole mobility because of the ionic impurity scattering effect [40]. Therefore, a higher mobility in the annealed GaSb indicated a reduction in the threading dislocation density of the GaSb layer, which was consistent with XRD ω scans. Unintentional p-type doping in the GaSb layer originated from multiple sources: 1) Ga anti-site, 2) Ga vacancy, and 3) threading dislocation-induced acceptors [29, 41]. A previous study used Deep Level Transient Spectroscopy (DTLS) to investigate the ex situ annealing GaSb on GaAs and indicated the signal of EL2 decreased after annealing [21]. The EL2 trap is associated with Ga anti-site [42], therefore, the annealing can suppress Ga anti-site. Ga vacancy (acceptor) transformed to Sb anti-site (donor) when the sample was annealed under Sb-rich conditions [43].

Annealed InSb also exhibited a higher mobility and lower concentration than as-grown InSb, which indicated a reduction in the defect density in the annealed InSb layer. Previous studies also demonstrated that the annealing process significantly decreased the threading dislocation density in the layer [19, 44]. The carrier mobility and concentration in the InSb layer on GaAs exhibited abnormalities in which both the mobility and concentration were lower at 77 K than at 300 K. Phonon scattering, a common carrier scattering mechanism, does not explain this phenomenon [45]. To investigate this phenomenon in detail, Figs. 6(a) and (b) show the temperature-dependent electron mobility and concentration in the as-grown and annealed InSb layers. The inset in Fig. 6 (a) is the mobility below 180 K, and the inset in Fig. 6(b) is the concentration from 150 to 300 K. For both samples, the highest mobility was achieved at 340 K. Above 340 K, the phonon scattering effect became the dominant mechanism, leading to decreasing mobility with increasing temperature. The carrier mobility was nearly unchanged at temperatures below 170 K and increased rapidly as the temperature increased from 170 to 340 K. In contrast, the concentration was nearly constant below 170 K, decreased from 170 to 250 K, and then increased rapidly above 250 K. The temperature dependent intrinsic electron concentration (n_i) in bulk InSb above 200 K

can be described using the following formula [46]:

$$n_i = 5.76 \times 10^{14} T^{1.5} \exp(-\frac{0.129}{k_B T}) \quad (2)$$

where k_B is the Boltzmann constant, T is the temperature, and k_BT is given in eV. The temperature dependent intrinsic concentration curve is shown in Fig. 6(b). The measured concentrations agreed well with the calculated value at temperatures above 250 K, but deviated from the calculated value at temperatures below 250 K. The intrinsic concentration was calculated to be around 10^{14} cm^{-3} in bulk InSb at temperatures less than 230 K, much lower than the measured concentration. To explain the behavior of the measured mobility and concentration, the effects of dislocations near the InSb/GaAs should be considered [47].

The TEM images (Figs. 4 and 5) and the findings of a previous study illustrated high-density misfit and threading dislocations near the InSb/GaAs interface [14]. The area near the interface can be called the "dislocation region," and the other part of the InSb layer can be called the "bulk region." Dislocations acted as donors that provided extrinsic carriers (electrons) [48]. Therefore, a high density of extrinsic carriers existed in the "dislocation region." Due to the physical properties of InSb (i.e., a small electron effective mass and a large Bohr radius for the donor), these extrinsic carriers formed an impurity band below the Fermi level, which is a feature of a degenerated semiconductor [49, 50]. In contrast, the "bulk region" is not expected to have an impurity band due to its relatively low dislocation density. The mobility and concentration values in this region are closer to those in the bulk InSb layer.

Therefore, the InSb layer on GaAs can be considered as a combination of a low-defect density InSb bulk layer (the bulk region) and a degenerated InSb buffer layer (the dislocation region). Below 230 K, most carriers were located in the "dislocation region," and the temperature dependent carrier concentration demonstrated behavior similar to that of a degenerated semiconductor, which has been confirmed by both simulations and experiments [49]. Above 230 K, the intrinsic carriers in the "bulk region," mentioned previously using Eq. (2), became dominant. As a result, the measured mobility began to exhibit the properties of a normal InSb bulk layer. Below 250 K, defect-generated extrinsic carriers in the "dislocation region" became dominant as the intrinsic carrier became negligible, leading to a low carrier mobility [51]. The measured carrier

mobility below 150 K (as shown in the inset in Fig. 6(a)) demonstrated a very slow increase as the temperature increased, which was attributed to the increasing thermal velocities of the carriers [52]. The rapid growth in mobility from 150 to 340 K was related to the transition of the dominant carrier-conducting region from the "dislocation region" to "bulk region." A detailed explanation can be found elsewhere [14]. Because this anomalous temperature dependent carrier mobility and concentration depends on both the dislocations near the InSb/GaAs interface and the intrinsic physical properties of InSb, therefore, this phenomenon is not found in the GaSb on GaAs mentioned above due to the higher electron effective mass in GaSb [53].

Another important application of GaSb and InSb materials is infrared photodetection. The 300 K wavelength dependent photoresponses of the as-grown and annealed GaSb photoconductors at the DC bias voltage of 0.5 V are shown in Fig. 7(a). The inset in Fig. 7(a) is an optical microscopic image of a GaSb-based photoconductor, in which an interdigitate electrode consists of 11 strip-shaped electrodes with 15.5 μm gaps between them. The annealed and as-grown photoconductors demonstrated similar shape of spectra response from 1.2 to 2.3 μm where a platform exhibited from 1.2 to 1.6 μm and a sharp decline exhibited in responsivity at the cutoff wavelength of approximately 1.6 μm. For the flat curve from 1.2 to 1.6 μm, the annealed photoconductor demonstrated a 6.9% higher responsivity than the as-grown one. The magnitude of responsivity is an indication of the material's minority carrier lifetime. Therefore, a high responsivity in the annealed device indicated an improvement in material quality. The cutoff wavelength is near the 300 K band gap energy of GaSb (0.724 eV). The downward slope in the annealed photoconductor is about -4.97 ($\frac{dR}{d\lambda}$), where R is relative responsivity (a.u.) and λ is wavelength (μm). The downward slope is the as-grown photoconductor is about -4.84, therefore, the downward slope is steeper in the annealed photoconductor. The electrical fields of the charged defects broaden the absorption edge of the semiconductors [54]. Thus, a steep decline in spectral responsivity indicated a lower density of defects in the annealed sample.

Fig. 7(b) shows the 77 K photoresponsivity of the as-grown and annealed InSb photoconductors at a DC bias voltage of 0.5 V. The measurements were carried out with a tunable quantum cascade laser whose wavelength was tunable from 4.3 to 6.6 μm with a resolution of 0.1 μm. Like the GaSb photoconductor, the annealed InSb photoconductor showed about 24.6% greater responsivity than the as-grown sample from 4.3 μm to 5.2 μm. The cutoff wavelength (~5.5 μm) was consistent with

the 77 K band gap energy of InSb (0.23 eV). The downward slope in the responsivity ($\frac{dR}{d\lambda}$) in the annealed photoconductor is -2.13, while, the slope in the as-grown one is -1.55. The steeper downward slope in responsivity for the annealed sample than for the as-grown sample indicates an improvement in the material quality in the annealed InSb layer.

The 77 K, 120 K, and 160 K responsivities of the annealed InSb photoconductor were also measured at DC applied voltages from 0 to 4 V. The results are shown in the inset of Fig. 7(b). The photocurrent increases linearly with the increase in applied voltage because the photoconductive gain is proportional to the transit time of the carriers that can be enhanced in the electrical field [55]. A noticeable increase in photocurrent is observed with the decrease in temperature, which is a result of the decrease in the numbers of thermally activated carriers and a longer carrier lifetime [56]. The photocurrent signal became undetectable above 220 K due to excessive high dark current.

4. Conclusions

In conclusion, GaSb and InSb samples were successfully grown on (100) GaAs substrates using an IMF array. The samples were annealed at different durations. The annealed samples demonstrated a lower surface roughness and defect density than the as-grown samples. The optimal annealing duration for GaSb and InSb were 5 minutes and 15 minutes, respectively. TEM observation and x-ray RSM indicated a stable IMF array and the absence of interfacial diffusion or rearrangement at the III-Sb/GaAs interfaces after the annealing process. The annealed samples exhibited greater carrier mobility by Hall measurement. The annealed III-Sb photoconductors consistently demonstrated greater photoresponsivity than the as-grown samples.

Acknowledgements

This work was supported by Singapore National Research Foundation through the Competitive Research Program (Grant No: NRF-CRP6-2010-4). The authors of this paper would like to express their gratitude to Dr. Liang Guozhen, Dr. Tong Jinchao and Mr. Zheng Yi for their assistance in photoconductor measurement and discussion.

References

[1] P.S. Dutta, H.L. Bhat, V. Kumar, The physics and technology of gallium antimonide: An emerging optoelectronic material, J. Appl. Phys. , 81 (1997) 5821-5870.
[2] Y.M. Sun, W.J. Jiang, M.C. Wu, Optical properties of GaSb alloys and photodiodes grown by liquid-phase epitaxy, J. Appl. Phys. , 80 (1996) 1731-1734.
[3] C. Downs, T.E. Vandervelde, Progress in Infrared Photodetectors Since 2000, Sensors-Basel, 13 (2013) 5054-5098.
[4] K.H. Tan, B.W. Jia, W.K. Loke, S. Wicaksono, S.F. Yoon, Formation of interfacial misfit dislocation in GaSb/GaAs heteroepitaxy via anion exchange process, J. Cryst. Growth 427 (2015) 80-86.
[5] I. Kimukin, N. Biyikli, T. Kartaloglu, O. Aytur, E. Ozbay, High-speed InSb photodetectors on GaAs for Mid-IR applications, IEEE J. Sel. Top. Quantum Electron. , 10 (2004) 766-770.
[6] V. Pusino, C.Z. Xie, A. Khalid, M.J. Steer, M. Sorel, I.G. Thayne, D.R.S. Cumming, InSb Photodiodes for Monolithic Active Focal Plane Arrays on GaAs Substrates, IEEE Trans. Electron Devices 63 (2016) 3135-3142.
[7] S.M. Ting, E.A. Fitzgerald, Metal-organic chemical vapor deposition of single domain GaAs on Ge/GexSi1-x/Si and Ge substrates, J. Appl. Phys. , 87 (2000) 2618-2628.
[8] H. Tanoto, S.F. Yoon, W.K. Loke, E.A. Fitzgerald, C. Dohrman, B. Narayanan, M. T Doan, C.H. Tung, Growth of GaAs on vicinal Ge surface using low-temperature migration-enhanced epitaxy, J Vac Sci Technol B, 24 (2006) 152-156.
[9] S.H. Huang, G. Balakrishnan, A. Khoshakhlagh, A. Jallipalli, L.R. Dawson, D.L. Huffaker, Strain relief by periodic misfit arrays for low defect density GaSb on GaAs, Appl. Phys. Lett. , 88 (2006).
[10] S.H. Huang, G. Balakrishnan, D.L. Huffaker, Growth Mode and Defect Evaluation of GaSb on GaAs Substrate: A Transmission Electron Microscopy Study, Journal of Nanoscience and Nanotechnology, 11 (2011) 5108-5113.
[11] K.C. Nunna, S.L. Tan, C.J. Reyner, A.R.J. Marshall, B.L. Liang, A. Jallipalli, J.P.R. David, D.L. Huffaker, Short-Wave Infrared GaInAsSb Photodiodes Grown on GaAs Substrate by Interfacial Misfit Array Technique, IEEE Photonics Technol. Lett. , 24 (2012) 218-220.
[12] B.C. Juang, R.B. Laghumavarapu, B.J. Foggo, P.J. Simmonds, A. Lin, B.L. Liang, D.L. Huffaker, GaSb thermophotovoltaic cells grown on GaAs by molecular beam epitaxy using interfacial misfit arrays, Appl. Phys. Lett. , 106 (2015).
[13] B.W. Jia, K.H. Tan, W.K. Loke, S. Wicaksono, S.F. Yoon, Formation of periodic interfacial misfit dislocation array at the InSb/GaAs interface via surface anion exchange, J. Appl. Phys. , 120 (2016) 035301.
[14] B.W. Jia, K.H. Tan, W.K. Loke, S. Wicaksono, S.F. Yoon, Effects of surface reconstruction on the epitaxial growth of III-Sb on GaAs using interfacial misfit array, Appl. Surf. Sci. , (2016).
[15] K.-M. Ko, J.-H. Seo, D.-E. Kim, S.-T. Lee, Y.-K. Noh, M.-D. Kim, J.-E. Oh, The growth of a low defect InAs HEMT structure on Si by using an AlGaSb buffer layer containing InSb quantum dots for dislocation termination, Nanotechnology, 20 (2009) 225201.
[16] H.-C. Luan, D.R. Lim, K.K. Lee, K.M. Chen, J.G. Sandland, K. Wada, L.C. Kimerling, High-quality Ge epilayers on Si with low threading-dislocation densities, Appl. Phys. Lett. , 75 (1999) 2909-2911.
[17] L. Colace, G. Masini, G. Assanto, H.-C. Luan, K. Wada, L. Kimerling, Efficient high-speed near-infrared Ge photodetectors integrated on Si substrates, Appl. Phys. Lett. , 76 (2000) 1231-1233.
[18] J.W. Lee, H. Shichijo, H.L. Tsai, R.J. Matyi, Defect Reduction by Thermal Annealing of Gaas-Layers Grown by Molecular-Beam Epitaxy on Si Substrates, Appl. Phys. Lett. , 50 (1987) 31-33.
[19] T. Sasaki, N. Oda, Dislocation Reduction in Hgcdte on Gaas by Thermal Annealing, J. Appl. Phys. , 78 (1995) 3121-3124.
[20] N. Hayafuji, T. Kimura, N. Yoshida, N. Kaneno, M. Tsugami, K. Mizuguchi, T. Murotani, S. Ibuki, Improvement of Inp Crystal Quality on Gaas Substrates by Thermal Cyclic Annealing, Jpn J Appl Phys 2, 28 (1989) L1721-L1724.
[21] M. Aziz, J.F. Felix, D. Jameel, N. Al Saqri, F.S. Al Mashary, H.M. Alghamdi, H.M.A. Albalawi, D. Taylor, M. Henini, Rapid thermal annealing: An efficient method to improve the electrical properties of tellurium compensated Interfacial Misfit GaSb/GaAs heterostructures, Superlattices Microstruct. , 88 (2015) 80-89.

[22] M. Aziz, A. Mesli, J.F. Felix, D. Jameel, N. Al Saqri, D. Taylor, M. Henini, Effect of post-growth annealing treatment on interfacial misfit GaSb/GaAs heterostructures, J. Cryst. Growth 424 (2015) 5-10.
[23] A. Craig, A. Marshall, Z.-B. Tian, S. Krishna, A. Krier, Mid-infrared InAs0. 79Sb0. 21-based nBn photodetectors with Al0. 9Ga0. 2As0. 1Sb0. 9 barrier layers, and comparisons with InAs0. 87Sb0. 13 pin diodes, both grown on GaAs using interfacial misfit arrays, Appl. Phys. Lett. , 103 (2013) 253502.
[24] E. Plis, J.-B. Rodriguez, G. Balakrishnan, Y. Sharma, H. Kim, T. Rotter, S. Krishna, Mid-infrared InAs/GaSb strained layer superlattice detectors with nBn design grown on a GaAs substrate, Semicond. Sci. Technol. , 25 (2010) 085010.
[25] D. Long, Photovoltaic and photoconductive infrared detectors, in: Optical and infrared detectors, Springer, 1980, pp. 101-147.
[26] A. Kurtz, S. Kulin, B. Averbach, Effect of dislocations on the minority carrier lifetime in semiconductors, Phys. Rev., 101 (1956) 1285.
[27] N.G. Weimann, L.F. Eastman, D. Doppalapudi, H.M. Ng, T.D. Moustakas, Scattering of electrons at threading dislocations in GaN, J. Appl. Phys. , 83 (1998) 3656-3659.
[28] M. Yamaguchi, M. Tachikawa, Y. Itoh, M. Sugo, S. Kondo, Thermal annealing effects of defect reduction in GaAs on Si substrates, J. Appl. Phys. , 68 (1990) 4518-4522.
[29] Y.B. Li, Y. Zhang, Y.W. Zhang, B.Q. Wang, Z.P. Zhu, Y.P. Zeng, Molecular beam epitaxial growth and characterization of GaSb layers on GaAs (001) substrates, Appl. Surf. Sci. , 258 (2012) 6571-6575.
[30] M.A. Moram, M.E. Vickers, X-ray diffraction of III-nitrides, Rep. Prog. Phys. , 72 (2009).
[31] T.A. Lafford, B.K. Tanner, P.J. Parbrook, Direct measurement of twist mosaic in GaN epitaxial films as a function of growth temperature, J Phys D Appl Phys, 36 (2003) A245-A248.
[32] A. Jallipalli, G. Balakrishnan, S.H. Huang, A. Khoshakhlagh, L.R. Dawson, D.L. Huffaker, Atomistic modeling of strain distribution in self-assembled interfacial misfit dislocation (IMF) arrays in highly mismatched III-V semiconductor materials, J. Cryst. Growth 303 (2007) 449-455.
[33] H.J. Gao, W.D. Nix, Surface roughening of heteroepitaxial thin films, Annu. Rev. Mater. Sci. , 29 (1999) 173-209.
[34] H.L. Tsai, J.W. Lee, Defect Structures at the Gaas/Si Interface after Annealing, Appl. Phys. Lett. , 51 (1987) 130-132.
[35] D. Lee, M. Park, Z. Tang, H. Luo, R. Beresford, C. Wie, Characterization of metamorphic In x Al 1− x As∕Ga As buffer layers using reciprocal space mapping, J. Appl. Phys. , 101 (2007) 063523.
[36] B.W. Jia, K.H. Tan, W.K. Loke, S. Wicaksono, S.F. Yoon, Epitaxial growth of low threading dislocation density InSb on GaAs using self-assembled periodic interfacial misfit dislocations, Mater. Lett. , 158 (2015) 258-261.
[37] M. De Giorgi, A. Taurino, A. Passaseo, M. Catalano, R. Cingolani, Interpretation of phase and strain contrast of TEM images of In x Ga 1− x A s/G a A s quantum dots, Phys. Rev. B, 63 (2001) 245302.
[38] L. Dong, J. Schnitker, R.W. Smith, D.J. Srolovitz, Stress relaxation and misfit dislocation nucleation in the growth of misfitting films: A molecular dynamics simulation study, J. Appl. Phys. , 83 (1998) 217-227.
[39] H. Matsuura, K. Morita, K. Nishikawa, T. Mizukoshi, M. Segawa, W. Susaki, Acceptor densities and acceptor levels in undoped GaSb determined by free carrier concentration spectroscopy, Jpn J Appl Phys 1, 41 (2002) 496-500.
[40] W. Zhou, X. Li, S.J. Xia, J. Yang, W. Tang, K.M. Lau, High Hole Mobility of GaSb Relaxed Epilayer Grown on GaAs Substrate by MOCVD through Interfacial Misfit Dislocations Array, Journal of Materials Science & Technology, 28 (2012) 132-136.
[41] M. Ichimura, K. Higuchi, Y. Hattori, T. Wada, N. Kitamura, Native Defects in the Alxga1-Xsb Alloy Semiconductor, J. Appl. Phys. , 68 (1990) 6153-6158.
[42] V. Virkkala, V. Havu, F. Tuomisto, M.J. Puska, Native point defect energetics in GaSb: Enabling p-type conductivity of undoped GaSb, Phys. Rev. B, 86 (2012) 144101.
[43] H. Bracht, S. Nicols, W. Walukiewicz, J.P. Silveira, Large disparity between gallium and antimony self-diffusion in gallium antimonide, Nature, 408 (2000) 69.
[44] H.C. Luan, D.R. Lim, K.K. Lee, K.M. Chen, J.G. Sandland, K. Wada, L.C. Kimerling, High-quality

Ge epilayers on Si with low threading-dislocation densities, Appl. Phys. Lett. , 75 (1999) 2909-2911.
[45] K. Hess, Impurity and phonon scattering in layered structures, Appl. Phys. Lett. , 35 (1979) 484-486.
[46] R. Cunningham, J. Gruber, Intrinsic Concentration and Heavy-Hole Mass in InSb, J. Appl. Phys. , 41 (1970) 1804-1809.
[47] A. Okamoto, I. Shibasaki, Transport properties of Sn-doped InSb thin films and applications to Hall element, J. Cryst. Growth 251 (2003) 560-564.
[48] Y.A. Osipyan, Y.I. Fedyaev, Donor Action of Dislocations in Insb, Jetp Lett-Ussr, 9 (1969) 21-&.
[49] J.J. Harris, T. Zhang, W.R. Branford, S.K. Clowes, M. Debnath, A. Bennett, C. Roberts, L.F. Cohen, The role of impurity band conduction in the low temperature characteristics of thin InSb films grown by molecular beam epitaxy, Semicond. Sci. Technol. , 19 (2004) 1406-1410.
[50] F. Stern, R.M. Talley, Impurity Band in Semiconductors with Small Effective Mass, Phys. Rev., 100 (1955) 1638-1643.
[51] E. Conwell, V.F. Weisskopf, Theory of Impurity Scattering in Semiconductors, Phys. Rev., 77 (1950) 388-390.
[52] F. Seitz, D.L. Dexter, Effects of Dislocations on Mobilities in Semiconductors, Phys. Rev., 87 (1952) 189-190.
[53] N. Bouarissa, H. Aourag, Effective masses of electrons and heavy holes in InAs, InSb, GaSb, GaAs and some of their ternary compounds, Infrared Phys Techn, 40 (1999) 343-349.
[54] D. Redfield, Effect of defect fields on the optical absorption edge, Phys. Rev., 130 (1963) 916.
[55] B.R. Conley, A. Mosleh, S.A. Ghetmiri, W. Du, R.A. Soref, G. Sun, J. Margetis, J. Tolle, H.A. Naseem, S.-Q. Yu, Temperature dependent spectral response and detectivity of GeSn photoconductors on silicon for short wave infrared detection, Opt. Express 22 (2014) 15639-15652.
[56] Z.-M. Liao, Y. Lu, J. Xu, J.-M. Zhang, D.-P. Yu, Temperature dependence of photoconductivity and persistent photoconductivity of single ZnO nanowires, Applied Physics A: Materials Science & Processing, 95 (2009) 363-366.

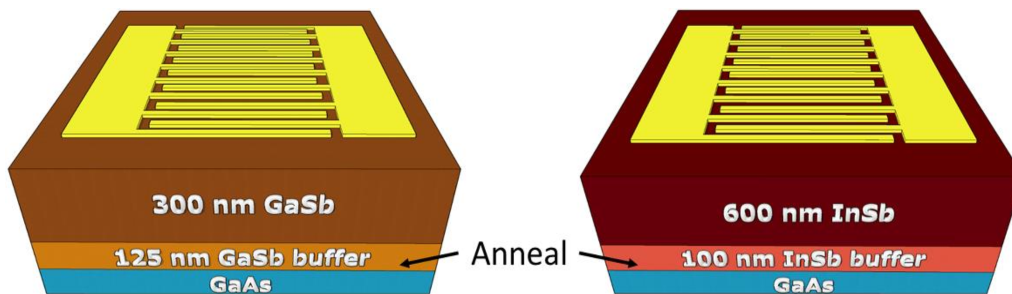

Fig. 1. Schematics of GaSb- and InSb-based photoconductors grown on (100) GaAs substrates.

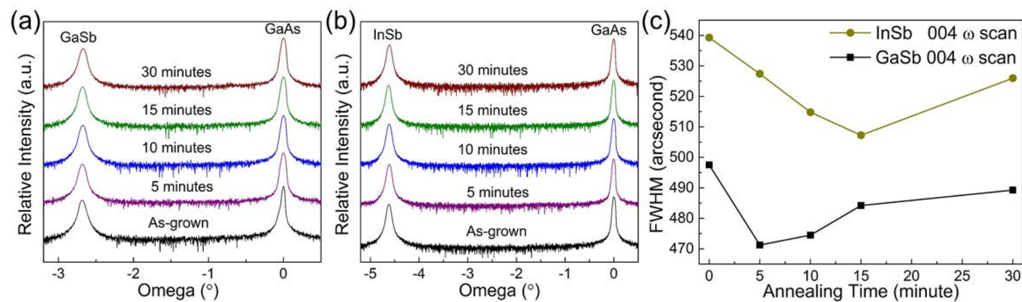

Fig. 2. Symmetric (004) XRD scan of III-Sb on GaAs. (a) & (b) symmetric (004) ω-2θ scans for GaSb and InSb, respectively. The annealing times are indicated; (c) The annealing time dependent

full-width-half-maximum (FWHM) from (004) rocking curve of GaSb and InSb.

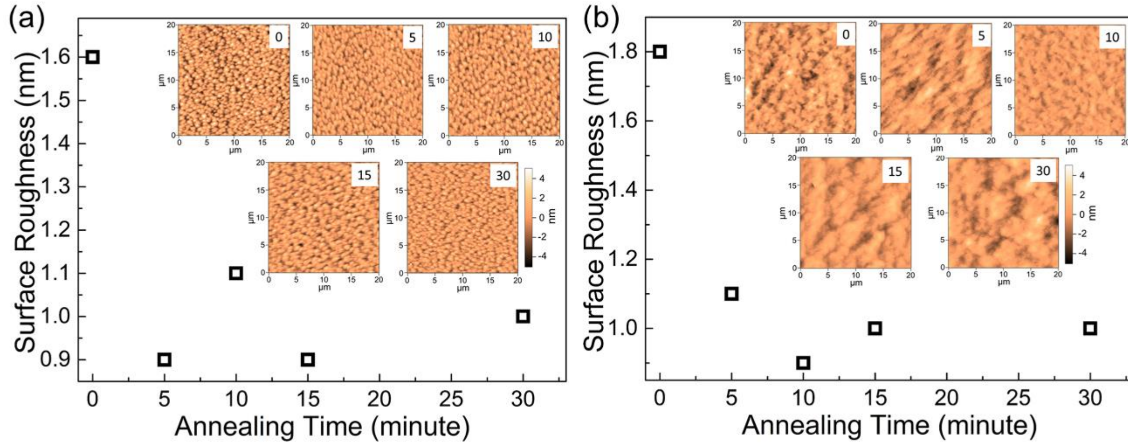

Fig. 3. Annealing time dependent r. m. s. surface roughness for III-Sb layers on GaAs. The insets are AFM images (20 μm × 20 μm) for samples with different annealing times. (a) GaSb on GaAs; (b) InSb on GaAs.

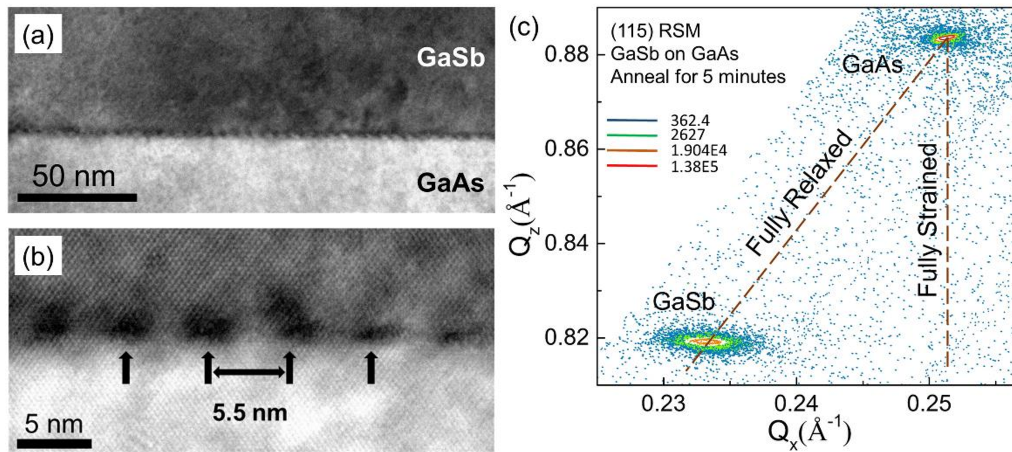

Fig. 4. Cross-sectional TEM images and x-ray RSM of the GaSb grown on GaAs with annealing for 5 minutes. (a) Bright field image; (b) High resolution TEM image where the interfacial misfit array is indicated by black arrows; (c) Asymmetric (115) RSM where reciprocal lattice GaSb peak positions for fully relaxed and strained epitaxial layer on GaAs are indicated by dashed lines, respectively.

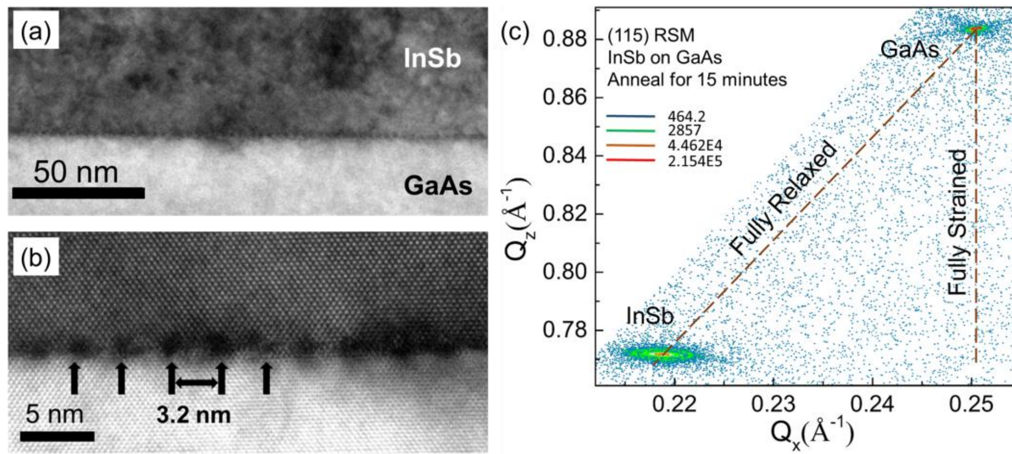

Fig. 5. Cross-sectional TEM images and x-ray RSM of the InSb grown on GaAs with annealing for 15 minutes. (a) Bright field image; (b) High resolution TEM image where the interfacial misfit array is indicated by black arrows; (c) Asymmetric (115) RSM where reciprocal lattice InSb peak positions for fully relaxed and strained epitaxial layer on GaAs are indicated by dashed lines, respectively.

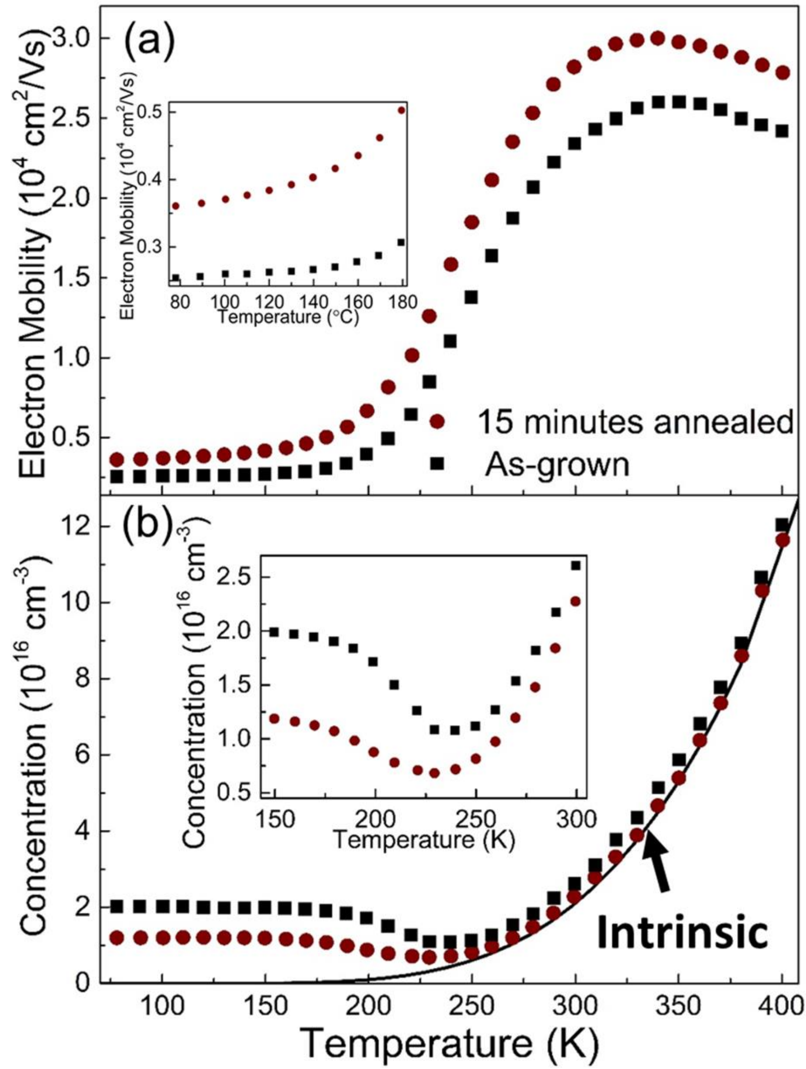

Fig. 6. Temperature dependence of (a) electron mobility and (b) concentration of as-grown and annealed InSb on GaAs. The inset in (a) shows mobility below 180 K. The inset in (b) shows concentration between 150 K and 300 K. The solid black line indicates the intrinsic electron concentration calculated by Eq. (2).

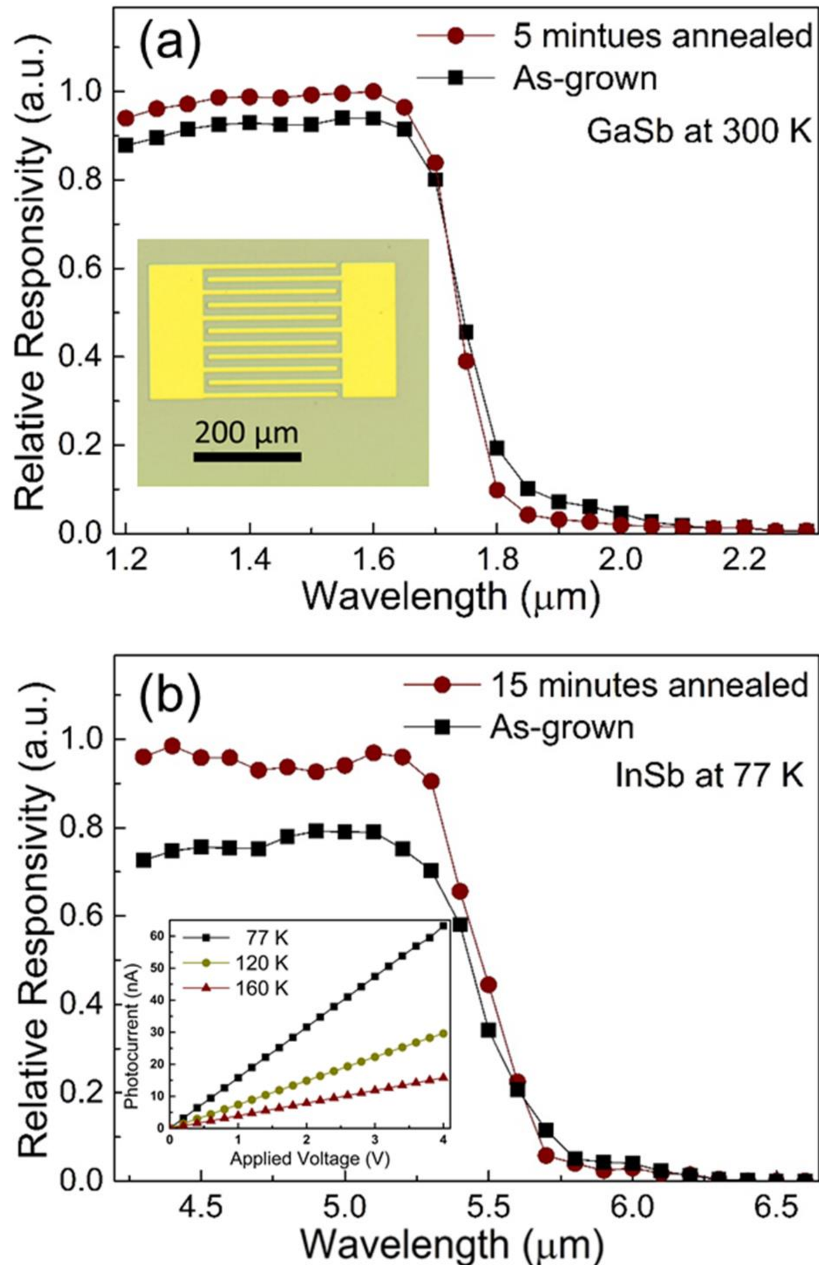

Fig. 7. Plot of DC relative responsivity vs wavelength for the as-grown and annealed (a) GaSb- and (b) InSb-based photoconductors at applied voltage of 0.5 V. The temperatures of measurement are 300 K for GaSb and 77 K for InSb. The inset in (a) is optical image of GaSb-based photoconductor. The inset in (b) is responsivity vs applied voltage for the annealed InSb-based photoconductor at 77 and 140 K.